


Accumulation of amyloid beta (A β) and amyloid precursor protein (APP) in tumors formed by a mouse xenograft model of inflammatory breast cancer

Astrid Zayas-Santiago¹, Michelle M. Martínez-Montemayor², Jadier Colón-Vázquez¹, Gabriela Ortiz-Soto², Jose G. Cirino-Simonet² and Mikhail Inyushin¹ 

¹ Department of Physiology, Universidad Central del Caribe, Bayamón, PR, USA

² Department of Biochemistry, Universidad Central del Caribe, Bayamón, PR, USA

Keywords

inflammatory breast cancer; xenografts; tumor; amyloid beta; immunostaining

Correspondence

M. Inyushin, Department of Physiology, Universidad Central del Caribe Ave. Laurel #100, Santa Juanita, Bayamón, PR 00956, USA

Tel: +1787 798 3001 ext. 2063

E-mail: mikhail.inyushin@ucaribe.edu

(Received 27 July 2021, revised 16 September 2021, accepted 29 October 2021)

doi:10.1002/2211-5463.13308

Edited by Miguel De la Rosa

Accumulation of amyloid in breast cancer is a well-known phenomenon, but only immunoglobulin light-chain amyloidosis (AL) or transthyretin (TTR) amyloid had been detected in human breast tumor samples previously. We recently reported that another amyloidogenic peptide, amyloid beta (A β), is present in an aggregated form in animal and human high-grade gliomas and suggested that it originates systemically from the blood, possibly generated by platelets. To study whether breast cancers are also associated with these A β peptides and in what form, we used a nude mouse model inoculated with triple-negative inflammatory breast cancer cell (SUM-149) xenografts, which develop noticeable tumors. Immunostaining with two types of specific antibodies for A β identified the clear presence of A β peptides associated with (a) carcinoma cells and (b) extracellular aggregated amyloid (also revealed by Congo red and thioflavin S staining). A β peptides, in both cells and in aggregated amyloid, were distributed in clear gradients, with maximum levels near blood vessels. We detected significant presence of amyloid precursor protein (APP) in the walls of blood vessels of tumor samples, as well as in carcinoma cells. Finally, we used ELISA to confirm the presence of elevated levels of mouse-generated A β 40 in tumors. We conclude that A β in inflammatory breast cancer tumors, at least in a mouse model, is always present and is concentrated near blood vessels. We also discuss here the possible pathways of A β accumulation in tumors and whether this phenomenon could represent the specific signature of high-grade cancers.

Inflammatory breast cancer (IBC) is one of the most aggressive types of this disease; it is highly metastatic and usually fatal (as it is commonly diagnosed at T4, according to the tumor–nodes–metastasis classification of cancers (TNM) classification). Various IBC carcinoma cell

subtypes exist, with the triple-negative subtype the most frequently diagnosed. These tumors lack receptors for estrogen, progesterone, or human epidermal growth factor receptor 2 (proto-oncogene) (HER2/neu), and thus, IBC is often treated with chemotherapy, radiation, or

Abbreviations

AD, Alzheimer's disease; AL, light-chain amyloidosis; APP, amyloid precursor protein; A β , amyloid beta; DAPI-4', 6-diamidino-2-phenylindole; ELISA, enzyme-linked immunosorbent assay; HER2/neu, human epidermal growth factor receptor 2 (proto-oncogene); IBC, inflammatory breast cancer; SUM-149-IBC cell line; MALT, mucosa-associated lymphoid tissue; MAPK, mitogen-activated protein kinases; PDGF, platelet-derived growth factor; SCID, severe combined immunodeficient (mice strain); TNM, tumor–nodes–metastasis classification of cancers; TTR, transthyretin.

surgery, due to the lack of targeted therapies. While IBC incidence is about 2%–5% of all breast cancers (with 70% higher occurrence in African American and younger women), it develops rapidly, accounting for 10% of breast cancer deaths annually in the United States [1,2]. Histologically, IBC has specific features of inflammation, with pathological evidence of cancer that includes increased angiogenesis and high infiltration of tumor-associated (immune-suppressing) macrophages involving tumor emboli in dermal-lymphatic vessels by large clusters of circulating tumor cells [3,4]. It was found that IBC-type carcinoma cells produce elevated levels of vascular endothelial growth factor, combining angiogenesis with enhanced vessel porosity [5]. Studying the expression of proteins important for breast cancer diagnostics in order to find specific markers of IBC enabled the discovery of elevated E-cadherin [6] and P-cadherin (cadherin signaling pathways control invasion and metastasis) expression in IBC tumors [7], but they are present in some non-IBC tumors as well. Besides cadherin, no unique genomic marker has been conclusively identified for IBC; thus, no specific molecular therapeutic approaches have yet been proposed to manage IBC [8]. Therefore, finding specific markers for high-grade breast cancers, such as IBC, became a recognized priority.

Recently, statistically independent cohort studies have found an inverse association between cancers in general (including breast cancer) and Alzheimer's disease (AD; [9–13]). These findings suggest that there are common factors in these diseases. Possible linkages in this cancer–AD relationship have been proposed: decreased mitochondrial metabolism, in general, and decreased signaling through the p53, Pin1, and Wnt cellular signaling pathways, in particular [9,14]. Besides these, the buildup of amyloid precursor protein (APP), the precursor of the AD hallmark amyloid beta (A β) peptides, has been discovered in breast cancer tumors and corresponding metastatic lymph nodes [15]. Initially, it was found that the proteolytic cleavage of APP by the α -secretase (non-amyloid) pathway reduces proliferation and migration in breast cancer [16]. Later, it was confirmed that APP controls breast cancer through the mitogen-activated protein kinases (MAPK) signaling pathway, regulating different kinases and the expression of filaments such as cadherins, cytokeratins, and vimentin. Generally, it was shown that APP overexpression increases the migratory and invasive ability of human breast cancer cells, whereas APP silencing significantly inhibits cell migration and invasion [17]. It was also discovered that APP has differential expression in different breast cancer cell lines, with triple-negative breast cancer cell lines having the highest level of APP expression [16]. We found no

published evidence on whether APP is cleaved to form A β peptides in breast cancer.

It was reported that A β peptide levels in blood plasma are significantly elevated in esophageal cancer, colorectal cancer, hepatic cancer, and lung cancer patients as well as in melanoma and adenocarcinoma [18–20]. We recently reported that A β is expressed in glioma cells and in close proximity to blood vessels in mouse and human late-stage glioma tumors [21,22]. Do IBC tumors also contain A β peptides, what is the source of this A β , and in what form does it take in IBC?

While it is known that APP is present in IBC, we found no published evidence on whether APP is cleaved to form A β peptides and aggregated A β amyloid in breast cancer. However, besides carcinoma cells themselves, another blood-related systemic source of A β peptide production may lead to its accumulation in tumors [23,24]. Recently, we found that platelets trigger a massive release of A β after thrombosis and that this release is concentrated near blood vessels [25,26]. It is known that platelets in cancer patients are hyperactivated and form cancer cell-induced aggregates and micro-thrombi in the vasculature near tumors. Poor survival in a large variety of cancers, including metastatic breast cancer, is associated with high platelet count, with thrombocytopenia or antiplatelet drugs reducing the short-term risk of cancer, cancer mortality, and metastasis [27]. Thus, platelet count may be a prognostic marker for breast cancer [28,29]. Previously, it was suggested that platelets affect cancer cells by releasing platelet-derived growth factor (PDGF; [30]). However, it was recently shown that A β oligomers inhibit the growth of various human cancer cells, including breast carcinoma cells [31]. Thus, there is the possibility that platelet-generated A β is produced in response to cancer development and released in tumors, as we suggested previously [24].

It is known that rarely (only in 7% of cases) aggregated amyloid, predominantly light-chain amyloidosis (AL) or sometimes misfolded transthyretin (TTR)-type amyloid, are detected in human breast tumor samples [32–37]. In patients with breast cancer and AL-type amyloid, over half have concurrent breast hematologic disorders [35,38].

In our study, we chose specific antibodies against A β peptides with low reactivity for its precursor APP to see whether A β immunoreactivity is present in xenograft tumors induced by triple-negative inflammatory breast cancer cells. In addition, the presence of APP itself was assessed in the same tumor tissues in general as well as in tumor blood vessels. The presence of aggregated forms of amyloid inside tumors was

evaluated using fluorescence histochemistry staining with dyes selective for aggregated β -pleated sheet amyloid. We also assessed whether $A\beta$ immunoreactivity and aggregated amyloid are concentrated near blood vessels.

Results

Immunoreactivity against $A\beta$ peptides and APP is present in all studied tumor samples but not in control skin samples

Triple-negative inflammatory breast cancer cell (SUM 149) tumors that were developed over 10 weeks after xenograft subcutaneous inoculations of hairless severe combined immunodeficient (SCID) mice were harvested, as described previously [39]. A total of three tumors from different animals were sliced and analyzed. Applying immunocytochemistry, we found that all tumor samples had both APP and $A\beta$ staining in a majority of the carcinoma cells (Fig. 1B,C, yellow arrows). It was also found that APP is specifically concentrated in the endothelial cells of blood vessels (Fig. 1C, white arrow). Interestingly, the $A\beta$ -specific antibody MOAB-2, reactive against $A\beta$ residues 1–4 and which recognizes both murine and human $A\beta$

peptide, stained not only carcinoma cells and some endothelial cells but also extracellular amyloid, most probably in fibrillary or aggregated form (Fig. 1B). The same amyloid was stained with 4',6-diamidino-2-phenylindole (DAPI, Fig. 1A), which is a fluorescent dye that binds to DNA and normally stains only the cell nucleus at visible levels. It was reported previously that DAPI specifically stains amyloid light-chain (AL) aggregates (while not labeling type A amyloid [AA]; [40]). Similarly, DAPI was reported to stain $A\beta$ plaques as well, although this finding was unpublished (ResearchGate, 2014) [41]. Thus, aggregated amyloid in xenograft tumors is either (a) pure $A\beta$ amyloid or (b) composed of mixed amyloids containing both $A\beta$ (stained with MOAB-2) and AL aggregates (stained with DAPI).

Control staining of healthy skin shows no visible presence of $A\beta$ and APP under the same recording conditions (Fig. S1).

Specific histochemical staining against β -sheet amyloid was present in all studied tumor samples but not in control skin samples

Slices from the same tumor samples were stained using Congo red and thioflavin S, both dyes known

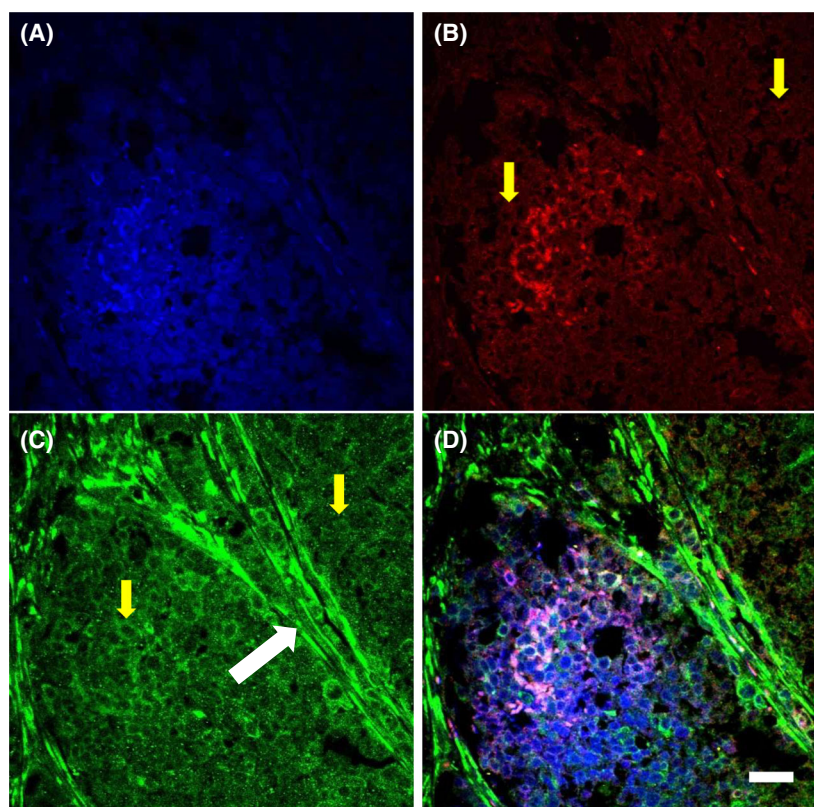


Fig. 1. Carcinoma cells have both $A\beta$ and APP immunoreactivity. (A) DAPI (blue); (B) $A\beta$ immunoreactivity (MOAB-2, red); (C) APP immunoreactivity (green); (D) A + B + C (overlay). Scale bar, 20 μ m; arrows, see text.

as specific fluorescent stains for aggregated β -pleated sheet amyloid [22,42–45]. Both Congo red (Fig. 2A1, A2) and thioflavin S (Fig. 2B1, B2) clearly stained carcinoma cells, which are recognizable because of their relatively similar shape and size. In addition, in adipose tissue attached to the tumor, some carcinoma cells fluorescently stained with thioflavin S can be seen around blood vessels (Fig. 2B2, yellow arrow). While the majority of carcinoma cells were stained with dyes, the staining was not uniform. Certain zones were obviously stained with slightly enhanced fluorescence (Fig. 2A2, B1, white arrows). We interpreted these enhancements as additional aggregated extracellular amyloid, but it may also be that in some carcinoma cells amyloid is concentrated. Similarly, the immunostaining of tumor carcinoma cells was also not uniform (Fig. 1). Previously, in studying glioma tumors we found that cells near blood vessels had enhanced amounts of $A\beta$ [21]. We hypothesized that amyloid is concentrated in specific places because of nearby blood vessels and that blood is the source of $A\beta$ (at least partially). Therefore, we analyzed the corresponding confocal brightfield images of blood vessels.

Specific staining with $A\beta$ amyloid antibodies (staining all forms of $A\beta$) and with Congo red/thioflavin S (against β -pleated sheet $A\beta$) is concentrated near blood vessels

Brightfield images clearly indicated blood vessel boundaries (Fig. 3A1, B1, white arrows) allowing us to measure the distance from the blood vessel to a tissue. We used corresponding fluorescence images of stained tissue, either with antibodies against $A\beta$ or with a histochemical stain against β -pleated sheet amyloid (example shown in Fig. 3A,B). IMAGEJ software (<https://imagej.nih.gov/ij/>) was applied, allowing us to measure the mean fluorescence level at particular loci at various distances from nearby blood vessels. This procedure allowed us to construct a graph of the dependence of $A\beta$ -related fluorescence (F , in arbitrary units) on the distance from blood vessels (in μm ; Fig. 3C). It was confirmed that $A\beta$ immunofluorescence is concentrated near blood vessels. A total of five slides with Congo red and $A\beta_{40-42}$ staining were analyzed, and the values near blood vessels appeared to be greater than at a distance of 30 μm or more (t -test: $t = 9.535$, $df = 8$, $P < 0.001$ for Congo red;

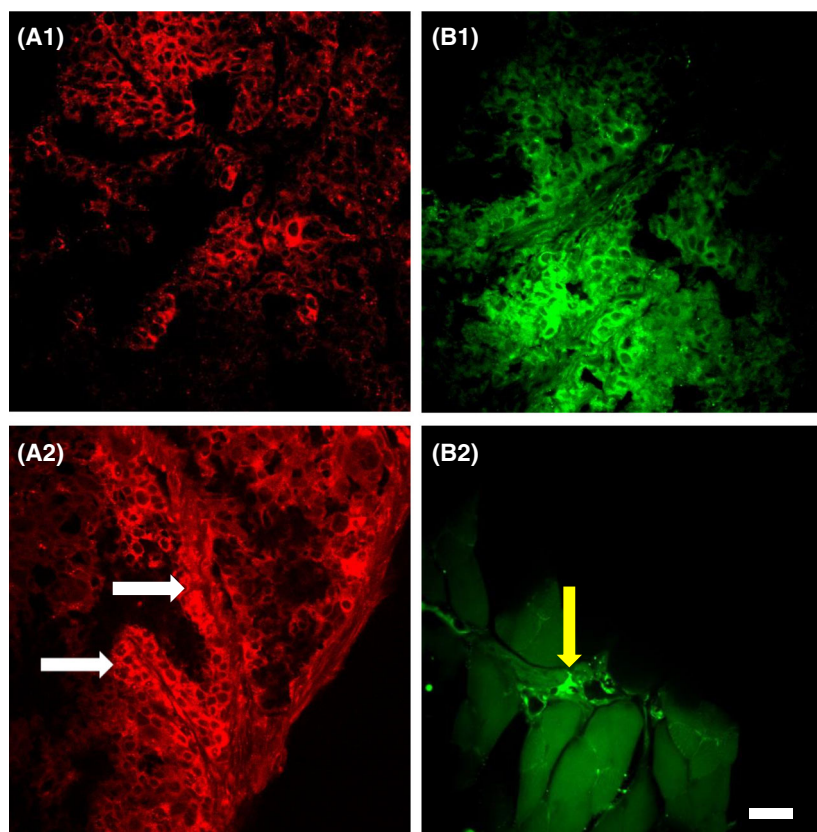


Fig. 2. Carcinoma stained with Congo red (A1, A2, red) and thioflavin S (B1, B2, green). Some zones have enhanced fluorescence (white arrows). Carcinoma cells in adipose tissue (yellow arrow). Scale bar, 20 μm .

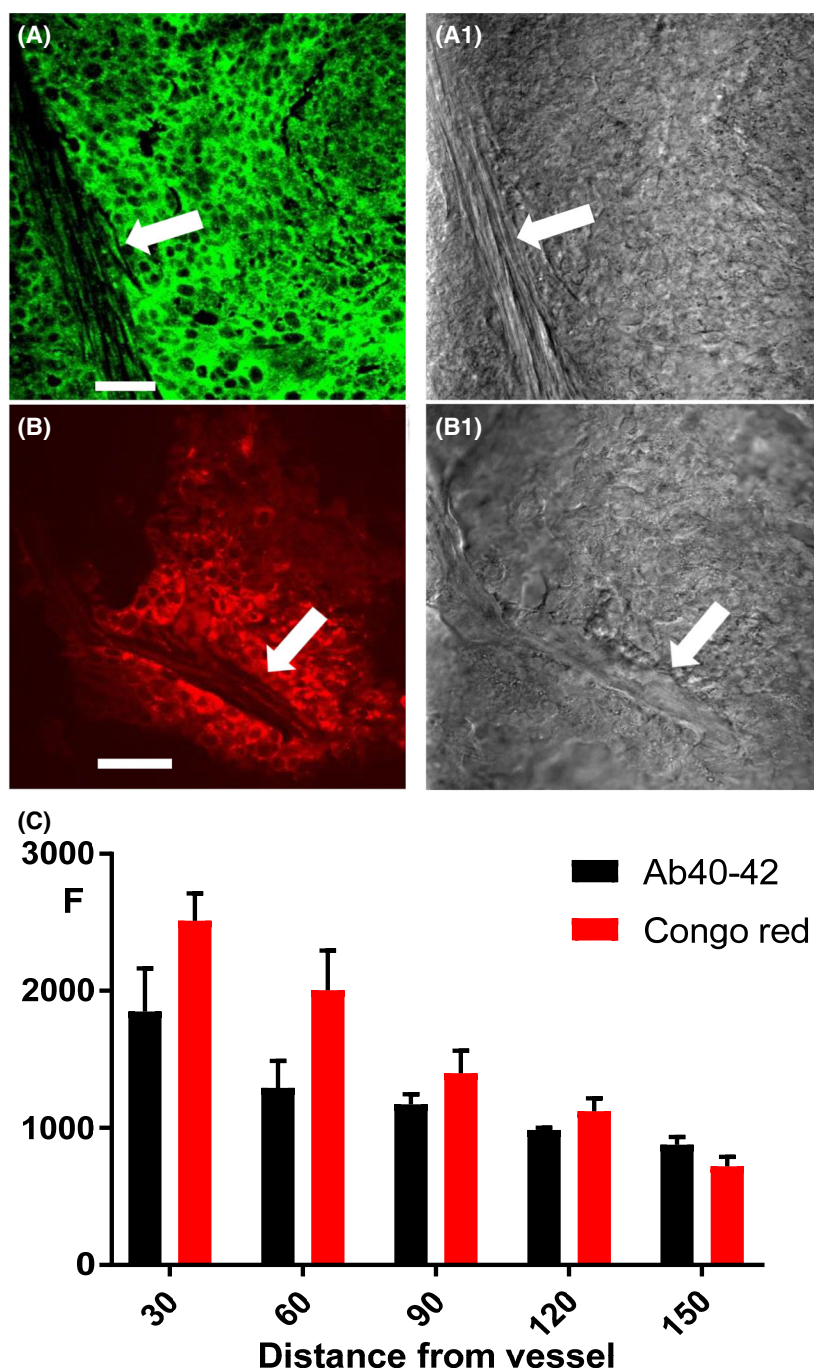


Fig. 3. Tumor tissue stained with a A β 1–42 polyclonal antibody reactive with A β 40 and 42 (A, green) and Congo red (B, red). The corresponding confocal brightfield images (A1 and B1) outline blood vessel boundaries (white arrows). A plot (C) shows the fluorescence level (F) at different distances (in μm) from blood vessels; error bars represent SD. Scale bar, 25 μm .

$t = 3.216$, $df = 8$, $P = 0.012$ for A β 40–42). It was then determined that levels of A β immunofluorescence and β -pleated sheet amyloid staining were effectively correlated (correlation coefficient 0.9549, $P < 0.01$). Thus, we confirmed that blood vessels are important for A β distribution in breast cancer tissue (see also the S3 video). Interestingly, DAPI staining was also concentrated in the vicinity of blood vessels (Fig. S2). We

ascribe this to the propensity of DAPI to stain aggregated amyloid.

Murine A β 40 is elevated in studied tumor samples

In our histochemical studies, we used pan-specific antibodies recognizing A β peptides from different species.

Because A β in xenograft tumors may have both a murine (systemic) and/or human (produced by human cancer cells) origin, we used a commercially available mouse-specific enzyme-linked immunosorbent assay (ELISA) kit to see whether systemic mouse A β 40 is concentrated in tumors. According to the manufacturer, this mouse A β 40 ELISA kit is very specific, and mouse A β 40 had no cross-reactivity with human A β 40 even till 10 ng·mL⁻¹. This allowed us to compare the freshly frozen samples from the xenograft tumors and controls. Measurements indicate that mean concentrations of mouse A β 40 peptides in tumors (1240 \pm 149.8, pg·mL⁻¹) versus controls (316.7 \pm 14.53, pg·mL⁻¹) are increased about fourfold ($P < 0.05$, $t = 6.136$, $df = 4$).

Discussion

We used two different specific antibodies against to visualize A β peptide distribution in inflammatory breast cancer SCID mouse model xenografts. It was found that both (a) MOAB-2 monoclonal antibodies specific for residues 1–4 of A β (with low affinity for APP) and (b) A β 1–42 polyclonal antibodies specific for the amino acid sequence at A β 40–42 specifically stain carcinoma cells (Figs 1B and 3A). Additionally, some aggregated forms of amyloid were stained. MOAB-2 antibodies stained these aggregates or filaments, but they were outlined by DAPI as well (Fig. 1A,B,D). It was reported previously that DAPI specifically stains amyloid light chain (AL) aggregates (while not staining AA; [40]). In addition, DAPI was described to stain A β plaques as well, although these results were not published [41]. Because there is no published evidence of DAPI staining of A β aggregates, there are two possibilities; aggregated amyloid in xenograft tumors is (a) pure A β amyloid or (b) a mixture of amyloid containing both A β (stained with MOAB-2) and AL aggregates (stained with DAPI).

Amyloid aggregates were also detected using fluorescence histochemical methods. We used two different amyloid-specific fluorescent dyes (Congo red and thioflavin S). Fluorescence detection of samples allows improved detection of amyloid in cytology preparations [45–47].

Using both dyes, we found intensive staining of amyloid in an aggregated form, especially near blood vessels (Figs 2A, panels A1 and B1, also 3B and S3 GIF video). While we also detected aggregated amyloid with A β immunostaining (Fig. 1), it is uncertain whether it is the only component of these aggregates.

Previous reports have established that aggregated amyloid in the breast is mainly of the AL type (usually κ light chain); in half of patients, it is part of an additional systemic immune cell disease, and in 55% of

patients, it is associated with a hematologic malignancy of the breast (usually mucosa-associated lymphoid tissue (MALT) lymphoma; [35,36]). By definition, L-amyloidosis is produced by the kappa light chain of immunoglobulin M (IgM). However, there is no literature investigating L-type amyloid in nude SCID mice. While the nude mouse model that we used is immunocompromised, IgM levels are usually unchanged (unlike other immunoglobulins) and similar to the levels of IgM in wild-type mice [48]. This finding suggests that L-type amyloid may be present in this mouse strain as well. Thus, amyloid in xenograft tumors may be of mixed type, and this question needs further study.

Carcinoma cells were also stained with antibodies against different isoforms of APP, but most distinctively anti-APP antibody marked blood vessel walls within the tumor (Fig. 1C,D). The antibody we used does not specifically recognize species-specific APP, and the origin of APP in xenograft tumors is not well established. It was shown that the stroma and vessels supporting the growth of many types of xenograft tumors were of murine origin or possibly a mosaic [49–51]. It is known that human and murine APP have only 86% similarity, and specific antibodies can detect the difference [52,53]. To prove that A β within the tumor has at least a partial murine origin, we used mouse-specific ELISA to measure A β in tumors and controls. It was found that the concentration of mouse-originated A β 40 is significantly elevated (~ 4-fold) in tumors, which confirmed the possible systemic mouse origin of amyloid. Thus, the APP that we observed in tumor blood vessels may be of murine origin, while the carcinoma cells that were injected to form xenografts were of human origin. Of course, future specific experiments will show whether human APP and A β are also present in tumors and determine the presence or absence of other amyloidogenic peptides (including possibly AL). Also, we confirmed that visible amounts of the A β precursor APP are present in xenografts tumors. While APP buildup has been reported previously in breast cancer tumors and the corresponding metastatic lymph nodes [15], the presence of its β -secretase cleavage product, A β , was not reported. Moreover, according to the literature, APP has shown differential expression in different breast cancer cell lines. It was found that triple-negative breast cancer cell lines have the highest levels of APP expression [16]. These authors also discovered that if the proteolytic cleavage of APP is processed by α -secretase (the non-amyloid pathway), proliferation and migration in breast cancer are reduced [16]. It was found that APP overexpression increased the migratory and invasive ability of human breast cancer cells, whereas APP silencing significantly inhibited cell migration and invasion [17]. Based on the results presented here and in the literature, we

suggest that APP processing in the β -secretase pathway would augment cell migration. The implication is that A β production indicates only highly invasive breast cancers, such as IBC.

There have been speculations that APP affects carcinoma cell mobility through APP binding protein 2 (APPBP2), which is highly expressed in breast cancer (<https://www.genecards.org/cgi-bin/carddisp.pl?gene=APPBP2>). Unfortunately, the expression of this protein concerning invasive properties is not known.

We still do not know whether carcinoma cells themselves process APP to generate A β . We have discovered that both A β immunoreactivity and aggregated amyloid are concentrated near blood vessels (Fig. 3), suggesting that blood vessels are important for A β production. In addition, A β of murine origin is elevated in tumors, demonstrating the murine and probably blood-related source of these peptides. These results suggest that systemic production of A β is important for its accumulation in tumors, including in the aggregated form, although other sources may also be involved, including carcinoma cells themselves, since in a previous study we found that mouse A β alone does not produce aggregated amyloid [53]. We also found a similar A β accumulation in aggressive gliomas [21,22], which could represent a specific signature of high-grade cancers. One future direction will be the study of A β production by inflammatory breast cancer cells *in vitro*. Another important task will be to determine whether A β production in this kind of tumor can be regulated to inhibit growth and migration.

Conclusions

We confirmed that A β peptides in inflammatory breast cancer tumor xenografts are always present in visible amounts and are concentrated near blood vessels within the tumors. The tumors studied also showed a strong presence of aggregated amyloid containing A β . While we studied only a xenograft model of IBC, we suggest that A β is present in inflammatory breast cancers in general and may be used as a marker of these cancers, but this possibility must be further evaluated.

Materials and methods

Cell culture and mouse subcutaneous SUM-149 cell tumors

Cell culture

The patient-derived IBC cell line SUM-149 (BioIVT, Westbury, NY, USA) was cultured in Ham's F12 medium (Life Technologies, Carlsbad, CA, USA) with 10% fetal bovine serum (FBS), as previously described [54–56]. SUM-149 IBC

cells were seeded 1 : 3 in 10-cm plates. Once they reached 70% confluency, 3 mL of culture media was collected every 72 h from three plates, while regular media served as control. For total protein extraction, the cells were harvested with a cell scraper and lysed on ice using NP-40 lysis buffer containing one protease inhibitor tablet (Roche Diagnostics Corporation, Indianapolis, IN, USA). Cells were incubated for 10 min on ice and vortexed intermittently. Supernatants were collected after centrifugation [21,256 g (RCF), 4 °C, 10 min], and protein concentration was quantified using the Precision Red protein assay kit (Cytoskeleton, Inc., Denver, CO, USA), as described previously [54,56,57].

Mouse subcutaneous tumors

Female severe combined immunodeficient (SCID) mice (21 days of age) were purchased from Charles River Laboratories International Inc. (Wilmington, MA, USA) and housed under specific pathogen-free conditions. The mice received an autoclaved AIN 76-A phytoestrogen-free diet (Tek Global, Harlan Teklad, Madison, WI, USA) and water *ad libitum*. Cell inoculations were performed as previously described by us [39,56]. Briefly, SUM-149 cells (3.0×10^6 , 1 : 1 serum medium: Matrigel; BD Biosciences, San Jose, CA, USA) were injected into the fourth right mammary fat pad under isoflurane inhalation. Mice were weighed weekly, while tumor weights were obtained at the end of the study (10 weeks). This project was approved by the UCC Institutional Animal Care & Use Committee (IACUC, protocol #037-2021-15-01-PHA-IBC).

Tissue preparation and cryosectioning

Tumors were excised and fixed in a solution of 4% paraformaldehyde in phosphate-buffered solution (PBS: NaCl, 137 mM; KCl, 2.7 mM; Na₂HPO₄, 10 mM; KH₂PO₄, 1.8 mM; in distilled water at pH 7.4) and incubated overnight (16–24 h) in the same fixative solution. After incubation, the tissues were transferred to PBS. After rinsing the tissues three times for 10 min per rinse at room temperature (RT) in 5% sucrose in PBS with gentle rotation, the tissues were cryoprotected with increasing concentrations of sucrose in PBS, which were obtained by mixing 5% sucrose and 20% sucrose in ratios of 2 : 1, 1 : 1, and 1 : 2. For each ascending concentration of sucrose, the tissues were incubated for 30 min at RT, and the tissues were then incubated overnight first in 20% sucrose and then in 30% sucrose at 4 °C. After this step, the samples were stored at –80 °C or immediately prepared for cryosectioning. Tissues were sectioned at a thickness of 30 μ m using a cryostat (CM1860, Leica Biosystems, Wetzlar, Germany) at –23 °C.

Immunostaining, histochemistry, and fluorescence confocal microscopy

The slides were air-dried for 30 min and immunostained using a previously established protocol [22,58]. First,

sections were treated for 20 min with a permeabilization solution consisting of 0.03% Triton X-100 (Sigma-Aldrich, St. Louis, MO, USA) and 1% dimethyl sulfoxide (DMSO; MP Biomedicals, Santa Ana, CA, USA) in PBS under gentle agitation (40 rpm). Second, the sections were treated for 60 min with a blocking solution containing either 5% normal goat serum, 5% normal horse serum, or 5% rabbit normal serum (Vector Laboratories, Burlingame, CA, USA) and 2% w/v bovine serum albumin (BSA; Sigma-Aldrich) in the permeabilization solution. Following the blocking step, the sections were processed with antibodies against A β and APP. Slices were incubated with a mouse monoclonal antibody to A β (MOAB-2, 1 : 200; Abcam, Cambridge, MA, USA, cat. #ab126649), a rabbit polyclonal antibody to A β 1–42 (1 : 200; Abcam, cat. #ab216504), and a rabbit polyclonal antibody to APP (1 : 200; Abcam, cat. #ab15272), all incubated overnight at 4 °C. After three washes with permeabilization solution for 10 min, the samples were incubated with either secondary goat antibody to rabbit IgG conjugated to Alexa Fluor® 647 (1 : 400; Abcam, cat. #ab150083), secondary horse antibody to mouse IgG conjugated to Texas red® (1 : 400; Vector Labs, TI-2000), or secondary rabbit antibody to goat IgG conjugated to FITC (1 : 400; Vector Labs, FI-5000) with shaking for 2 h at room temperature and protected from light. The slices were then washed three times with PBS for 10 min and once with distilled water before being transferred onto a glass slide containing Fluoroshield™ mounting medium (Sigma-Aldrich, cat. #F6057) with DAPI.

For thioflavin staining, we used thioflavin S (Th-S). Human brain slices (30 μ m) containing tumors were completely air-dried before staining. The slides were washed twice with 450 μ L of 100% EtOH for 2 min each wash. Next, the slides were washed once with 450 μ L of 70% EtOH for 2 min then washed once with 450 μ L of 80% EtOH for 2 min. Finally, the slides were washed with 450 μ L of tap water, 450 μ L of distilled water, and 450 μ L of alkaline alcohol solution for 2 min each, then incubated for 5 min with Th-S. After incubation, the slides were washed with 450 μ L of tap water, then dehydrated with 450 μ L of 95% EtOH for 3 min and two changes of 450 μ L of 100% EtOH for 3 min each. The coverslip was mounted with a drop of Vectashield® mounting medium to visualize fluorescence (Vector Laboratories, Burlingame, CA, USA, cat. #H-1000).

Congo red staining was performed as follows. A 0.5% Congo red solution was prepared in 50% alcohol. Human brain slices (30 μ m) containing tumors were air-dried thoroughly and then washed twice with absolute alcohol for 2 min. The slides were washed twice with 450 μ L of 100% EtOH for 2 min each wash, followed by washing once with 450 μ L of 70% EtOH for 2 min, 450 μ L of 80% EtOH for 2 min, and 450 μ L of tap water and incubated for 20 min in a filtered solution of Congo red (0.2- μ m filter). After incubation, the slides were rinsed once with distilled water, incubated in 450 μ L of alkaline alcohol solution for 2 min, and then washed with 450 μ L of tap water. Finally, the slices were dehydrated with 450 μ L of 95% EtOH for 3 min, with two changes of 450 μ L of 100% EtOH for

3 min each. The glass slides were mounted with Fluoroshield mounting medium containing 4',6-diamidino-2-phenylindole (DAPI).

FITC excitation/emission filters were used to visualize specific amyloid-associated Th-S and a Texas-Red filter for Congo red fluorescence.

Images were acquired using an Olympus Fluoview FV1000 scanning inverted confocal microscope system equipped with 4x, 10x, 20x, or 40x/1.43 oil objectives (Olympus, Tokyo, Japan). The images were analyzed using IMAGEJ software (ver. 1.8.0_112, <http://imagej.nih.gov/ij>) with the Open Microscopy Environment Bio-Formats library and plugin (<http://www.openmicroscopy.org/site/support/bio-formats5.4/>), allowing for the opening of Olympus files. The images were evaluated using custom colorization.

Enzyme-linked immunosorbent assay measurements

A specialized, ready-to-use, mouse-specific, solid-phase sandwich ELISA kit (cat. #KMB3481; Invitrogen, Thermo Fisher Scientific, Waltham, MA, USA) was used for direct measurement of the amount of mouse A β 40 peptide in tumors and controls, as we described previously (Kucheryavych *et al.*, 2019) [21]. The tissue samples were homogenized mechanically, and 100 mg of homogenate from each sample was then lysed in guanidine solution (5 M guanidine HCl, 50 mM Tris/HCl, pH 8.0). A monoclonal antibody against the NH₂ terminus of mouse A β 40 was coated onto the wells of the microtiter strips provided in the kit. Samples, including standards of known A β 40 content for calibration purposes as well as experimental specimens, were pipetted into the wells. After washing, the rabbit antibody specific to the COOH terminus of A β 40 was added and detected with horseradish peroxidase-labeled anti-rabbit antibody. The optical density values at 450 nm were determined using a Wallac 1420 Victor2 microplate reader (PerkinElmer Inc., Waltham, MA, USA). A standard curve was used for final determination of the concentration of A β 40 in the samples and is presented as picograms of A β 40 per milliliter of initial homogenate.

Statistics and measurements

Using GRAPH PAD PRISM 7.03 (GraphPad Software, Inc., La Jolla, CA, USA) for calculations, an unpaired *t*-test was employed to estimate statistical differences. Values were determined to be significantly different if the two-tailed *P*-value was < 0.05.

Acknowledgements

This research was funded by the NIH, grant number SC2 GM111149 to MI and grant number SC3 GM111171 to MM. We want to acknowledge Dr.

Martinez and Dr. Zayas laboratory staff and students, for the excellent technical support. The funders had no role in the design of the study; in the collection, analyses, or interpretation of data; in the writing of the manuscript; or in the decision to publish the results.

Conflict of interest

The authors declare no conflict of interest.

Author contributions

MI, MM, and AZ conceptualized the study; AZ, MM, JC-V, JC-S, and GS contributed to methodology; MM, MI, and AZ validated the data; AZ made formal analysis; JC-V, JC-S, and GS contributed to data curation; MI involved in initial draft preparation; AZ, MM, MI, JC-V, JC-S, and GS reviewed and edited the manuscript; MM and AZ supervised the study; AZ, MM, and MI involved in project administration. All authors have read and agreed to the published version of the manuscript.

Data accessibility

The data that support the findings of this study are available in the supplementary material of this article.

References

- Hance KW, Anderson WF, Devesa SS, Young HA and Levine PH (2005) Trends in inflammatory breast carcinoma incidence and survival: the surveillance, epidemiology, and end results program at the National Cancer Institute. *J Natl Cancer Inst* **97**, 966–975.
- Abraham HG, Xia Y, Mukherjee B and Merajver SD (2021) Incidence and survival of inflammatory breast cancer between 1973 and 2015 in the SEER database. *Breast Cancer Res Treat* **185**, 229–238.
- Mu Z, Wang C, Ye Z, Austin L, Civan J, Hyslop T, Palazzo JP, Jaslow R, Li B, Myers RE *et al.* (2015) Prospective assessment of the prognostic value of circulating tumor cells and their clusters in patients with advanced-stage breast cancer. *Breast Cancer Res Treat* **154**, 563–571.
- Cserni G, Charafe-Jauffret E and van Diest PJ (2018) Inflammatory breast cancer: the pathologists' perspective. *Eur J Surg Oncol* **44**, 1128–1134.
- Gadde M, Phillips C, Ghousifam N, Sorace AG, Wong E, Krishnamurthy S, Syed A, Rahal O, Yankeelov TE, Woodward WA *et al.* (2020) In vitro vascularized tumor platform for modeling tumor-vasculature interactions of inflammatory breast cancer. *Biotechnol Bioeng* **117**, 3572–3590.
- Kleer CG, van Golen KL, Braun T and Merajver SD (2001) Persistent E-cadherin expression in inflammatory breast cancer. *Mod Pathol* **14**, 458–464.
- Ben Hamida A, Labidi IS, Mrad K, Charafe-Jauffret E, Ben Arab S, Esterni B, Xerri L, Viens P, Bertucci F, Birnbaum D *et al.* (2008) Markers of subtypes in inflammatory breast cancer studied by immunohistochemistry: prominent expression of P-cadherin. *BMC Cancer* **29**, 28.
- Chakraborty P, George JT, Woodward WA, Levine H and Jolly MK (2021) Gene expression profiles of inflammatory breast cancer reveal high heterogeneity across the epithelial-hybrid-mesenchymal spectrum. *Transl Oncol* **14**, 101026.
- Behrens MI, Lendon C and Roe CM (2009) A common biological mechanism in cancer and Alzheimer's disease? *Curr Alzheimer Res* **6**, 196–204.
- Rocca WA, Petersen RC, Knopman DS, Hebert LE, Evans DA, Hall KS, Gao S, Unverzagt FW, Langa KM, Larson EB *et al.* (2011) Trends in the incidence and prevalence of Alzheimer's disease, dementia, and cognitive impairment in the United States. *Alzheimer's Dement* **7**, 80–93.
- Driver JA, Beiser A, Au R, Kreger BE, Splansky GL, Kurth T, Kiel DP, Lu KP, Seshadri S and Wolf PA (2012) Inverse association between cancer and Alzheimer's disease: results from the Framingham Heart Study. *BMJ* **12**, e1442.
- Musicco M, Adorni F, Di Santo S, Prinelli F, Pettenati C, Caltagirone C, Palmer K and Russo A (2013) Inverse occurrence of cancer and Alzheimer disease: a population-based incidence study. *Neurology* **81**, 322–328.
- Ospina-Romero M, Glymour MM, Hayes-Larson E, Mayeda ER, Graff RE, Brenowitz WD, Ackley SF, Witte JS and Kobayashi LC (2020) Association between Alzheimer Disease and cancer with evaluation of study biases: a systematic review and meta-analysis. *JAMA Netw Open* **3**, e2025515.
- Sánchez-Valle J, Tejero H, Ibáñez K, Portero JL, Krallinger M, Al-Shahrour F, Tabarés-Seisdedos R, Baudot A and Valencia A (2017) A molecular hypothesis to explain direct and inverse co-morbidities between Alzheimer's Disease, Glioblastoma and Lung cancer. *Sci Rep* **7**, 4474.
- Tsang JYS, Lee MA, Ni YB, Chan SK, Cheung SY, Chan WW, Lau KF and Tse GMK (2018) Amyloid precursor protein is associated with aggressive behavior in nonluminal breast cancers. *Oncologist* **23**, 1273–1281.
- Tsang JYS, Lee MA, Chan TH, Li J, Ni YB, Shao Y, Chan SK, Cheung SY, Lau KF and Tse GMK (2018) Proteolytic cleavage of amyloid precursor protein by ADAM10 mediates proliferation and migration in breast cancer. *EBioMedicine* **38**, 89–99.
- Wu X, Chen S and Lu C (2020) Amyloid precursor protein promotes the migration and invasion of breast cancer cells by regulating the MAPK signaling pathway. *Int J Mol Med* **45**, 162–174.

- 18 Jin WS, Bu XL, Liu YH, Shen LL, Zhuang ZQ, Jiao SS, Zhu C, Wang QH, Zhou HD, Zhang T *et al.* (2017) Plasma amyloid-beta levels in patients with different types of cancer. *Neurotox Res* **2017**, 283–288.
- 19 Munir H, Jones JO, Janowitz T, Hoffmann M, Euler M, Martins CP, Welsh SJ and Shields JD (2021) Stromal-driven and Amyloid β -dependent induction of neutrophil extracellular traps modulates tumor growth. *Nat Commun* **12**, 683.
- 20 Kleffman K, Levinson G, Wong E, Galán-Echevarría F, Von-Itter R, Rose I, Blumenberg L, Alfredo Floristán A, James Tranos J, Argibay D *et al.* (2021) Melanoma-secreted amyloid beta suppresses neuroinflammation and promotes brain metastasis. *bioRxiv* 854885. <https://doi.org/10.1101/854885>
- 21 Kucheryavykh LY, Ortiz-Rivera J, Kucheryavykh YV, Zayas-Santiago A, Diaz-Garcia A and Inyushin MY (2019) Accumulation of Innate Amyloid Beta Peptide in Glioblastoma Tumors. *Int J Mol Sci* **20**, 2482.
- 22 Zayas-Santiago A, Díaz-García A, Nuñez-Rodríguez R and Inyushin M (2020) Accumulation of amyloid beta in human glioblastomas. *Clin Exp Immunol* **202**, 325–334. <https://doi.org/10.1111/cei.13493>
- 23 Inyushin MY, Sanabria P, Rojas L, Kucheryavykh Y and Kucheryavykh L (2017) A β peptide originated from platelets promises new strategy in anti-alzheimer's drug development. *Biomed Res Int* **2017**, 3948360.
- 24 Inyushin M, Zayas-Santiago A, Rojas L and Kucheryavykh L (2020) On the role of platelet-generated amyloid beta peptides in certain amyloidosis health complications. *Front Immunol* **11**, 571083.
- 25 Kucheryavykh LY, Dávila-Rodríguez J, Rivera-Aponte DE, Zueva LV, Washington AV, Sanabria P and Inyushin MY (2017) Platelets are responsible for the accumulation of β -amyloid in blood clots inside and around blood vessels in mouse brain after thrombosis. *Brain Res Bull* **128**, 98–105.
- 26 Kucheryavykh LY, Kucheryavykh YV, Washington AV and Inyushin MY (2018) Amyloid beta peptide is released during thrombosis in the skin. *Int J Mol Sci* **19**, 1705.
- 27 Jurasz P, Alonso-Escolano D and Radomski MW (2004) Platelet–cancer interactions: mechanisms and pharmacology of tumour cell-induced platelet aggregation. *Br J Pharmacol* **143**, 819–826.
- 28 Stravodimou A and Voutsadakis IA (2013) Pretreatment thrombocytosis as a prognostic factor in metastatic breast cancer. *Int J Breast Cancer* **2013**, 1–6.
- 29 Garmi N, Nasrallah S, Baram Y, Katz A, Koren A, First M and Blum A (2020) Platelets and breast cancer. *Isr Med Assoc J* **22**, 613–617.
- 30 Hermanson M, Funa K, Hartman M, Claesson-Welsh L, Heldin CH, Westermark B and Nistér M (1992) Platelet-derived growth factor and its receptors in human glioma tissue: expression of messenger RNA and protein suggests the presence of autocrine and paracrine loops. *Cancer Res* **52**, 3213–3219.
- 31 Pavliukeviciene B, Zentelyte A, Jankunec M, Valiuliene G, Talaikis M, Navakauskiene R, Niaura G and Valincius G (2019) Amyloid β oligomers inhibit growth of human cancer cells. *PLoS ONE* **14**, e0221563.
- 32 Fu K and Bassett LW (2001) Mammographic findings of diffuse amyloidosis and carcinoma of the breast. *AJR Am J Roentgenol* **177**, 901–902.
- 33 Röcken C, Kronsbein H, Sletten K, Roessner A and Bässler R (2002) Amyloidosis of the breast. *Virchows Arch* **440**, 527–535.
- 34 Chiang D, Lee M, Germaine P and Liao L (2013) Amyloidosis of the breast with multicentric DCIS and pleomorphic invasive lobular carcinoma in a patient with underlying Extranodal Castleman's disease. *Case Rep Radiol* **2013**, 1–3.
- 35 Said SM, Reynolds C, Jimenez RE, Chen B, Vrana JA, Theis JD, Dogan A and Shah SS (2013) Amyloidosis of the breast: predominantly AL type and over half have concurrent breast hematologic disorders. *Mod Pathol* **26**, 232–238.
- 36 Herrero L, Naranjo-Hans D, Solé M, Santamaría G, Bargalló X, Velasco M and Fernández PL (2015) Amyloidosis of the breast: three different and unusual presentations of a rare entity. *Pathobiology* **82**, 264–268.
- 37 Mori M, Kotani H, Sawaki M, Hattori M, Yoshimura A, Gondo N, Adachi Y, Kataoka A, Sugino K, Horisawa N *et al.* (2019) Amyloid tumor of the breast. *Surg Case Rep* **5**, 31.
- 38 Fischer EG (2020) Localized breast amyloidosis associated with sjögren syndrome. *Case Rep Pathol* **2020**, 8828263.
- 39 Suarez-Arroyo IJ, Rosario-Acevedo R, Aguilar-Perez A, Clemente PL, Cubano LA, Serrano J, Schneider RJ and Martínez-Montemayor MM (2013) Anti-tumor effects of Ganoderma lucidum (reishi) in inflammatory breast cancer in in vivo and in vitro models. *PLoS ONE* **8**, e57431.
- 40 Matsuura M, Abe H, Tominaga T, Sakurai A, Murakami T, Kishi S, Bando Y, Minakuchi J, Nagai K and Doi T (2017) A novel method of DAPI staining for differential diagnosis of renal amyloidosis. *J Med Invest* **64**, 217–221.
- 41 Researchgate. DAPI staying of amyloid beta plaques. Available online: <https://www.researchgate.net/post/Has-anyone-ever-noticed-DAPI-staying-the-beta-amyloid-plaques-in-brain-tissue>. Accessed May 7, 2021.
- 42 Puchtler H and Sweat F (1965) Congo red as a stain for fluorescence microscopy of amyloid. *J Histochem Cytochem* **13**, 693–694.
- 43 Sun A, Nguyen XV and Bing G (2002) Comparative analysis of an improved thioflavin-s stain, Gallyas silver stain, and immunohistochemistry for neurofibrillary

- tangle demonstration on the same sections. *J Histochem Cytochem* **50**, 463–472.
- 44 Marcus A, Sadimin E, Richardson M, Goodell L and Fyfe B (2012) Fluorescence microscopy is superior to polarized microscopy for detecting amyloid deposits in Congo red-stained trephine bone marrow biopsy specimens. *Am J Clin Pathol* **138**, 590–593.
 - 45 Clement CG and Truong LD (2014) An evaluation of Congo red fluorescence for the diagnosis of amyloidosis. *Hum Pathol* **45**, 1766–1772.
 - 46 Kelényi G (1967) Thioflavin S fluorescent and Congo red anisotropic stainings in the histologic demonstration of amyloid. *Acta Neuropathol* **7**, 336–348.
 - 47 Giordagze TA, Shiina N, Baloch ZW, Tomaszewski JE and Gupta PK (2004) Improved detection of amyloid in fat pad aspiration: an evaluation of Congo red stain by fluorescent microscopy. *Diagn Cytopathol* **31**, 300–306.
 - 48 Mink JG, Radl J, van den Berg P, Haaijman JJ, van Zwieten MJ and Benner R (1980) Serum immunoglobulins in nude mice and their heterozygous littermates during ageing. *Immunology* **40**, 539–545.
 - 49 Chang YS, di Tomaso E, McDonald DM, Jones R, Jain RK and Munn LL (2000) Mosaic blood vessels in tumors: frequency of cancer cells in contact with flowing blood. *Proc Natl Acad Sci USA* **97**, 14608–14613.
 - 50 Hylander BL, Punt N, Tang H, Hillman J, Vaughan M, Bshara W, Pitoniak R and Repasky EA (2013) Origin of the vasculature supporting growth of primary patient tumor xenografts. *J Transl Med* **11**, 110.
 - 51 Dong Z, Imai A, Krishnamurthy S, Zhang Z, Zeitlin BD and Nör JE (2013) Xenograft tumors vascularized with murine blood vessels may overestimate the effect of anti-tumor drugs: a pilot study. *PLoS ONE* **8**, e84236.
 - 52 Yamada T, Sasaki H, Furuya H, Miyata T, Goto I and Sakaki Y (1987) Complementary DNA for the mouse homolog of the human amyloid beta protein precursor. *Biochem Biophys Res Commun* **149**, 665–671.
 - 53 van Groen T, Kiliaan AJ and Kadish I (2006) Deposition of mouse amyloid beta in human APP/PS1 double and single AD model transgenic mice. *Neurobiol Dis* **23**, 653–662.
 - 54 Martínez-Montemayor MM, Ling T, Suárez-Arroyo IJ, Ortiz-Soto G, Santiago-Negrón CL, Lacourt-Ventura MY, Valentín-Acevedo A, Lang WH and Rivas F (2019) Identification of biologically active ganoderma lucidum compounds and synthesis of improved derivatives that confer anti-cancer activities in vitro. *Front Pharmacol* **10**, 115.
 - 55 Rios-Fuller TJ, Ortiz-Soto G, Lacourt-Ventura M, Maldonado-Martinez G, Cubano LA, Schneider RJ and Martínez-Montemayor MM (2018) Ganoderma lucidum extract (GLE) impairs breast cancer stem cells by targeting the STAT3 pathway. *Oncotarget* **9**, 35907–35921.
 - 56 Suárez-Arroyo IJ, Feliz-Mosquea YR, Pérez-Laspiur J, Arju R, Ghashuddin S, Maldonado-Martínez G, Cubano LA, Schneider RJ and Martínez-Montemayor MM (2016) The proteome signature of the inflammatory breast cancer plasma membrane identifies novel molecular markers of disease. *Am J Cancer Res* **6**, 1720–1740.
 - 57 Acevedo-Díaz A, Ortiz-Soto G, Suárez-Arroyo IJ, Zayas-Santiago A and Martínez Montemayor MM (2019) Ganoderma lucidum extract reduces the motility of breast cancer cells mediated by the RAC¹Lamellipodin axis. *Nutrients* **11**, 1116.
 - 58 Zayas-Santiago A, Agte S, Rivera Y, Benedikt J, Ulbricht E, Karl A, Dávila J, Savvinov A, Kucheryavykh Y, Inyushin M *et al.* (2014) Unidirectional photoreceptor-to-Müller glia coupling and unique K⁺ channel expression in Caiman retina. *PLoS ONE* **9**, e97155.

Supporting information

Additional supporting information may be found online in the Supporting Information section at the end of the article.

Fig. S1. (A) Ab1-40-control tissue; (B) MOAB-2 -control tissue; (C) Tioflavin S - control tissue; (D) Congo Red (red) - control tissue, Scale bar 20 μ m.

Fig. S2. DAPI staining of amyloid near blood vessels, Scale bar, 20 μ m.

Fig. S3. GIF video in which confocal Congo red fluorescence is concentrated near blood vessels. Original files from confocal microscope in TIFF format are present as zipped Supplementary Information files.